3D Mechanical Modeling of the GPS Velocity Field Along the Main Recent Fault and Kazerun Fault (Zagros, Iran)

H.R. Nankali[1], F. Sobouti[2], B. Voosoghi[3], K. Hessami[4], M. Talebian[5], A. Walpersdorf[6], and F. Tavakoli[7]

1. Research Associate, Khajeh Nasridin Toosi, University of Technology, Faculty of Geodesy and Geomatics Engineering and National Cartographic Center of Iran,Tehran, I.R. Iran, Email: nankali@ncc.org.ir
2. Assistant Professor, Institute for Advanced Studies in Basic Sciences, Department of Physics, Zanjan, I.R. Iran
3. Assistant Professor, Khajeh Nasridin Toosi, University of Technology, Faculty of Geodesy and Geomatics Engineering, Tehran, I.R. Iran
4. Assistant Professor, Seismology Research Center, International Institute of Earthquake Engineering and Seismology, Tehran, I.R. Iran
5. Research Associate, Research Institute of Earth Science, Geological Survey of Iran, Tehran, I.R. Iran
6. Associate Professor, Laboratoire de Géophysique Interne et Tectonophysique, CNRS, Université Joseph Fourier, France
7. Research Associate, National Cartographic Center of Iran, Geodesy and Geodynamics Department, Tehran, I.R. Iran

ABSTRACT: *The NW-SE trending Zagros mountains form a linear belt more than 1500km in length, from eastern Turkey in the NW to the strait of Hormuz in the SE. They result from the continental collision between the Arabian plate and Central Iran that started during the Miocene [e.g. 40], or perhaps earlier in Cenozoic time. A three-dimensional visco-elastic finite element model was developed in order to simulate long-term, displacement rate along the Main Recent Fault and Kazeun fault by adjusting the effective fault friction. In order to undertake this process, a friction range of 0.02-0.3 was used for a fault. A model was constructed using spatially varying crustal thickness, geothermal gradient, and two major faults. The mesh covers a rectangular area in the Zagros with horizontal dimensions of 1500km×600km and a depth extent of 70km. Structural boundaries are derived from several deep seismic soundings carried out in the area. The constructed model is first used in the calculation of thermal initial condition and secondly in analyzing the deformation. The structure of the fault zones is represented by contact surface with the Coulomb friction law. One of the most striking results of our rheological test is that the faults are locked if the friction exceeds 0.2. By comparing our results with geodetic measurements [48, 51], a realistic model is defined in which the displacement rates on the MRF and Dena, Kazerun and Borazjan faults reach 3.3mmyr^{-1}, 2.8mmyr^{-1}, 1.9mmyr^{-1}, 0.5mmyr^{-1} for a fault friction of 0.02. These results strongly suggest that MRF and Kazerun fault are weak faults like San Andreas and North Anatolian faults.*

Keywords: Zagros; Finite-element methods; Shortening; GPS; Iran; Rheology

1. Introduction

Two models have been proposed to describe accommodation of deformation in oblique convergence regions. In the first case, the normal and parallel velocities vary more or less linearly across the deformation zone [52] and in the second case, the deformation is partitioned into two components: the shortening component which is taken up by a dipping fault and the shear component, which occurs on a

subvertical strike-slip fault [15]. Another alternative which has been suggested to describe the active tectonic deformation is microplate behavior which assumes that the deformation is localized on faults bordering rigid blocks. This description is in good agreement with the present day velocity field of the Anatolian region [37] and of California [28]. Recent *GPS* studies in Zagros and Iran [21, 46, 48, 51] bring new data on the kinematics of continental deformation and specially in the Zagros region. The geodetic rate of Arabia-Eurasia convergence appears to be in good agreement with geological studies, suggesting a constant strain rate over at least the last 10*Ma* [29]. Meanwhile, *GPS* confirms the quasi-rigid behavior of the Central Iranian Block, which seems to be limited to the Sanandaj-Sirjan zone [22]. If the Arabia/ Eurasia collision rate seems to be steady over the last 10*Ma*, the tectonic has changed inside the collision zone and most of the present-day active faults are younger than 5*Ma* [1]. The goal of this study is to investigate the interaction between rheological properties of the Zagros crust and the displacement rate on the Main Recent fault and Kazerun fault, constraint by *GPS* and heat flow data, using a 3*D* mechanical model.

2. Tectonic Context

The tectonic setting of the Zagros is complicated by the Eurasia-Arabia collision, taking place entirely inside Iran's political borders. The current Eurasia-Arabia convergence rate increases from northwest to southeast along the Zagros from 18 to 25$mmyr^{-1}$ with an overall north-south orientation. This increase is due to the proximity of the Arabia-Eurasia Euler pole situated in North Africa at $27.9^{o} \pm 0.5^{o}N$, $19.5^{o} \pm 1.4^{o}E$ [48].

The Zagros mountain belt is approximately 1500*km* long, 250-400*km* wide, and runs from eastern Turkey where it connects to the North and East Anatolian faults, to the Oman Sea, where it dies out in the Makran subduction zone, see Figure (1). The belt lies on the former Arabian passive margin that is covered by up to 10*km* of Cambrian to Miocene sediments [17, 40, 41]. These sediments contain several layers of evaporate at different depths that decouple the surface deformation from that of the basement [6-8]. The late Cretaceous-early Miocene closure of Neo-Tethys between Arabia and Eurasia led to underthrusting of continental margin sediments along the Main Zagros Reverse Fault during the early stages of collision [40-41]. During the subsequent

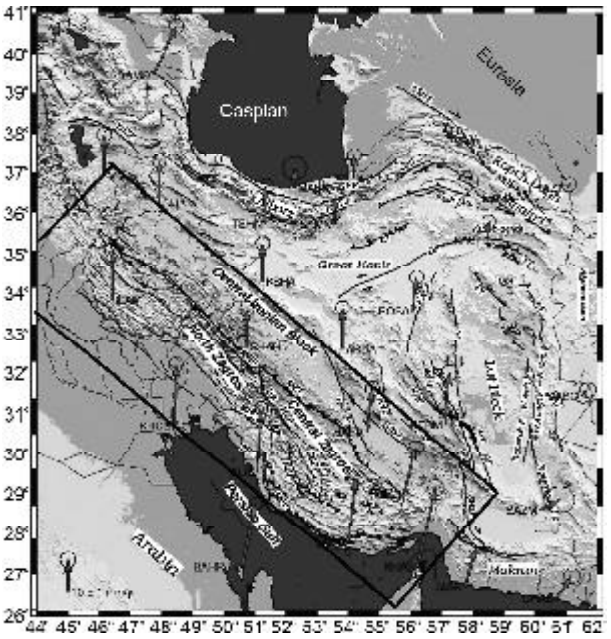

Figure 1. Framework of the Arabia-Eurasia collision in Iran. The arrows display the GPS velocity field as computed by Vernant et al [48]. Thin solid lines represent active faults and thick solid lines represent model boundaries.

continental convergence, the Zagros deformation front migrated southwestward [14, 20]. The current plate margin (the Zagros deformation front) can be defined by seismogenic thrusts in the basement, which underlie folds in the sedimentary cover representing mainly thin skinned shortening above the basement [14]. The main recent fault (*MRF*) is an active *NW-SE* trending right lateral strike-slip fault that runs *NW* of the *MZT* [7]. Using the offset of an Upper Cretaceous ophiolitic unit and of the major drainage Talebian and Jackson [44] obtain a value of 50*km*. Assuming that the right-lateral slip along the *MRF* was initiated 3 to 5*Myr* ago, they derived a strike-slip rate of about 10-17$mmyr^{-1}$. This is compatible with the estimate of 10$mmyr^{-1}$ of Bachmanov et al [4] based on the offset of a river valley incised into a surface of likely postglacial age.

Estimated slip rates of 16$mmyr^{-1}$ on the Main Recent fault calculated by Liu and Bird [27] is compatible with slip rates of 10-17$mmyr^{-1}$ Talebian and Jackson [44] but much larger than geodetic slip rates of 3±2$mmyr^{-1}$ Vernant et al [48] and Hessami et al [21].

Early studies of the Zagros using the earthquakes deeper than 50*km* is reported by the International Seismological Centre (*ISC*) and *US* Geological Survey (*USGS*) catalogues to postulate subduction of the continental Arabian shield beneath the Zagros [9, 18]. However, neither local seismograph networks, nor

modeling of teleseismic body waves from larger earthquakes has found any focal depths deeper than 15-20*km* [5, 13, 23, 47].

In the Zagros Mountains nearly all earthquakes are confined to the upper crust (depths <20*km*), and there is no evidence for a seismically active subducted slab dipping *NE* beneath central Iran, see Figure (2).

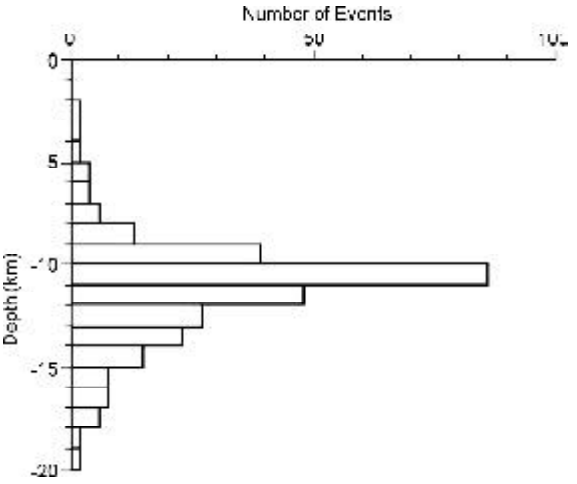

Figure 2. Earthquake depth distribution in Zagros [47].

3. Previous Studies

Studying the Zagros belt can be of great help to better understand the dynamics of mountain ranges. Published data on the Zagros crustal structure including moho depth estimates are very scarce. The only available profiles of crustal thickness variations have been computed from Bouguer anomaly modeling by Dehghani and Makris [12] for whole of Iran and Snyder and Barazangi [43] for Zagros. Hatzfeld et al [16] estimated a crustal thickness of 46*km* from receiver function computed at a single station close to the town of Ghir in central Zagros. The numerous seismic reflection profiles recorded for oil exploration do not penetrate the crust beyond the thick Hormuz salt layer at 9 to 12*km* depth [10, 29, 30, 39].

Analysis of the seismological network data across central Zagros by Paul et al [36] show Moho depth variations with a lateral resolution of a few km along a 620-km-long profile transverse to the range. The average crustal thickness is 45*km* beneath most of the Zagros fold-and-thrust belt and 42*km* beneath the Urumieh-Dokhtar volcanic zone and the southern part of the Iranian micro continent. The region between the suture zone in the High Zagros to the Sanandaj-Sirjan metamorphic zone is characterized by a marked crustal thickening from 45 to 70*km* in a narrow region.

Bird et al [9] reached similar conclusions using 2-*D* finite element modeling of lithospheric deformation in the Zagros assuming pure anelastic rheology. He showed that the shear stress concentrates on the suture zone for all slab-pull boundary conditions whatever the densities and flow laws considered.

The thin viscous sheet model has been applied to Iran [24, 41]. Both of these studies concluded that deformation of the Iranian lithosphere is determined by the shape of the rigid boundaries and the disposition of rigid blocks within the collision zone.

Vernant and Chéry [50] use a simple 2.5 *D* mechanical modeling for the Zagros and show that for the case of the *NW* Zagros, Main Recent Fault can accommodate only 25% of the whole tangential motion. As the *GPS* inferred range parallel motion across the *NW* Zagros is $5 mmyr^{-1}$, the present day slip rate of this fault could be as low as $1.2 mmyr^{-1}$. Their model shows that no strike-slip activity takes place on a vertical fault when the direction of convergence is more frontal. Vernant and Chéry [50] using a simple 2 layer numerical modeling with linear Maxwell rheology and rough elastic constant show that the mechanical behavior of the Iranian lithosphere seems to be partly controlled by the large strike slip faults. However, some deformation is still taken up by the continuum medium, suggesting a compromise between the micro plate and continuum descriptions.

Liu and Bird et al [27] use a kinematic finite-element method to derive a self-consistent long-term-average velocity field by combining space geodesy, geological slip rates and principal 'stress directions' (e.g. seismic moment tensor orientations) in Persia-Tibet and Burma Orogen. They show that Arabia-Eurasia relative plate motion in eastern Iran (east of 58°, *E*) is mainly accommodated by the Makran subduction zone and Kopet Dagh. Despite little constraint from input geological slip rates, their model predicts the correct sense (compared to earthquake focal mechanisms) for strike-slip faults on the west and east sides of the Lut block. The central Iran and Lut blocks appear to be relatively rigid, with strain localization on their boundary faults. West of 58°, *E*, Arabia-Eurasia convergence is accommodated by the Zagros and Alborz mountain ranges. Output slip rates of $16 mmyr^{-1}$ on the Main Recent fault are compatible with input slip rates of $10\text{-}17 mmyr^{-1}$ by Talebian and Jackson [44], but much larger than geodetic slip rates of $3\pm2 mmyr^{-1}$ by Vernant et al [48]. They suggest that a transition from strong to

weak coupling between the underthrusting Arabian plate and the Zagros in western Iran and Makran subduction in the east may affect surface deformation patterns in the Zagros and the Makran subduction zone. Previous numerical models of Zagros deformation have been constructed using the assumption of a continuum deformation, but without direct constraints on the velocity field and seismic data and structure in Zagros. In this study, a three-dimensional finite element model was used to account for the rheological properties of the Zagros lithosphere, including both pressure and temperature dependent rheological laws and fault discontinuities.

4. Model Setup

Finite element techniques are used to study lithospheric deformation and temperature evolution during time. The finite element method was chosen because it allows the calculation of stresses, strains and temperatures in compositionally heterogeneous models with non-linear rheologies and complex geometries.

All modeling presented here was conducted using the *ANYSYS* finite element program. *ANYSYS* employs the Newton-Raphson approach to solve nonlinear problems. In this method a load is subdivided into a series of increments applied over several steps. Before each solution the Newton-Raphson method evaluates the out-of-balance load vector, which is the difference between the restoring forces and the loads corresponding to the element stresses and the applied loads. A linear solution is performed using the out of balance loads and is checked for convergence. If convergence criteria are not satisfied the out-of balance load vector is reevaluated, the stiffness matrix updated and a through direct elimination of equations until the problem converges [33-35]. The program uses a Lagrangian formulation along with logarithmic (Hencky) strain and Cauchy (True) stress measure to describe the large deformation related to viscous flow [19]. This approach assumes that elastic strains are small relative to plastic strains and that viscous flow is incompressible. The solution to the elasto-perfectly plastic and thermally activated power-law creep material laws is achieved by an implicit algorithm. This scheme is unconditionally stable and the time step size is only constrained by the overall convergence and the desired accuracy of the calculations.

5. Model Geometry and Rheology

A finite element model was constructed to determine how the deformation is accommodated in Zagros with different rheologies in the lithosphere.

The model incorporates five key features:

(1) The Arabian plate moves towards the Eurasian plate at a rate of $22 mm yr^{-1}$ on a $N10^{o}\_E$ oriented vector [e.g., 32, 37, 38, 48]),

(2) The Zagros region is crossed by near-vertical strike-slip faults that cut through the crust [45, 51],

(3) The crustal velocity structure is known [16, 25, 35].

(4) The crustal geotherm is derived from thermal analysis of model,

(5) Geodetic observations constrain the rate of combined interseismic elastic and ductile strain.

The finite element model of the Zagros region was built in three compositional layers inferred from measured crustal velocity structure [16, 35]. Horizontal boundaries divide the crust into the upper and lower part. This division is approximately based on the P-wave velocity isolines for the boundary between the upper and the lower crust, and the Moho boundary for division between the crust and the mantle. We have tried to keep the model structurally as simple as possible and therefore the finest details found in the seismic velocity sections are excluded. Rock composition determines material elastic constants and, consequently, the strain response to an imposed stress at a given rate and temperature.

The finite element model is stratified, but as will be described, these layers do not necessarily show abrupt boundaries from elastic to viscoelastic behavior. The upper $20 km$ of the model represents the upper crust. Elastic properties of these rocks were approximated by wet granite and are given in Table (1). The lower crust is $28 km$ thick in the model and has elastic properties representative of basalt-diabase composition. The upper mantle layer has properties associated with mixed dry and wet dunite samples, see Table (1), and is $22 km$ thick.

All elements of the Zagros finite element model strained through a combination of linear elasticity and rate dependent creep behavior. Time-independent elastic strain occurred in the model according to

$$\varepsilon = \sigma / E \tag{1}$$

where E is Young's modulus and σ is differential stress.

Modeled time-dependent inelastic strain rate was controlled by the creep equation (e.g., [26])

$$d\varepsilon / dt = A exp(-Qc / RT)\sigma^{n} \tag{2}$$

Table 1. Material constants used in three layers of the finite element model.

Parameter	Layer 1		Layer 2		Layer 3	
	0-20km	Source	20-48km	Source	>48km	Source
E Young's Modulus, MPa	$6x10^4$	16	$9.4x10^4$	16	$1.6x10^5$	16
A Physical Constant, $MPa^{-n}S^{-1}$	$2x10^{-4}$	34	$6.3x10^{-2}$	34	$5x10^3$	34
n Power Law Exponent	1.9	34	3.1	34	3.8	34
Q Activation Energy, kJ/mo1	140.6	34	276	34	492	34
ν Poisson's Ratio	0.25	34	0.26	34	0.28	34
ρ Density$*10^3$kg/m^3	2.775	43	2.905	43	3.200	43

where *A* (elastic constant), *Qc* (activation energy), and *n* are experimentally derived elastic constants, *R* is the universal gas constant, *T* is temperature, and σ is differential stress, see Table (1).

Eq. (2) adds an important contribution to the modeled strain with increasing temperature and simulated a smooth transition from elastic to ductile strain with depth. At low temperatures the exponential term of Eq. (2) approached unity, causing the creep term to become vanishingly small. With increasing temperature, the contribution of the exponential term became more important.

The finite element model has cuts in it that represent two major strike-slip faults of the Zagros i.e Main Recent fault and Kazerun, see Figure (1). The faults are deformable and are constructed from contact elements that obey the Coulomb failure relation:

$$CF = \tau + \mu(\sigma_n) \qquad (3)$$

where τ is the shear stress acting on a fault surface, μ is the friction coefficient, and σ_n is the stress component normal to the fault surface. Contact elements have zero thickness and are welded to the sides of elements.

The properties of the contact surface can be controlled by the contact stiffness *K* and the coefficient of friction. The contact stiffness *K* can be envisaged as the stiffness of a spring that is put between two contacting areas when contact occurs. The amount of penetration between the two surfaces is therefore dependent on *K*. The coefficient of friction is a material property which in case of a fault, depends on the contacting materials, surface roughness and the existence of smearing fault gauge and clay minerals, among others. Thus, the coefficient of friction can vary over a wide range, i.e between 0.85 the typical value for intact rock and 0.18 if clay minerals are present [11].

The geothermal gradient input to the creep equation controls material behavior which the model elements behave according to Hook's law, see Eq. (1), where temperatures are low and become transitionally more viscous at higher temperatures.

Faults are permitted to extend down to the base of the model. The initial fault friction coefficients were set to a low value of 0.1 [50]. As shown, fault friction coefficients were modified slightly to match observed long-term rates and the displacement rate. Our mesh covers a rectangular area from south east to northwest Iran with horizontal dimensions of 1500*km*×600*km* and a depth extent of 70*km*, see Figure (3). The model is composed entirely of eight-node elements and consists of 28125 elements with 119260 active nodes.

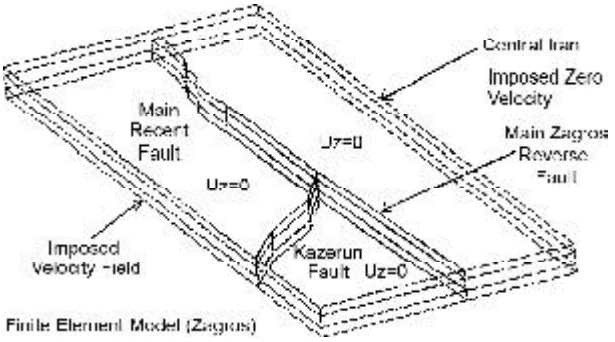

Figure 3. Model Geometry and Boundary conditions, see the text for more details.

Elements were defined by 8 nodes, each having 3 degrees of freedom (translations in the nodal *x, y*, and *z* directions). All elements in this study had capability of elastic and inelastic deformation, with inelastic strain behavior defined by a rate-dependent creep relation. The mesh is finest where volumes change shapes the most, and in regions of greatest complexity such as fault terminations or intersections.

6. Physical Parameters

Physical parameters are chosen so that they are representative of typical rock types occurring in the continent including felsic composition for the upper crust, mafic for the lower crust and ultra mafic for the mantle. We have approximated these compositions with creep parameters, see Table (1). Material parameter variation has been kept to a minimum in horizontal directions. Elastic material parameters, i.e.,Young's Modulus and Poisson's ratio are taken from the ratio of P- and S-wave velocities along seismic profiles [42] and were used to confine the Poisson's ratio, see Table (1). Values of densities are taken from the velocity models of seismic profiles and from the gravity model of Synder and Barazangi [43] for the Zagros profile, see Table (1).

A simplification is made, as densities are kept constant in each horizontal layer, i.e., in the upper crust $2775 kgm^{-3}$, in the lower crust $2950 kgm^{-3}$, and in the mantle $3200 kgm^{-3}$. Thermal conductivity follows the temperature dependence [18] with different starting values in the crust and in the mantle, see Table (2). Values of the heat production vary in the upper crust between $1.5\text{-}2\ \mu Wm^{-3}$ and in the lower crust between $0.2\text{-}0.5\ \mu Wm^{-3}$. In the mantle, values ranging from 0 to $0.02\ \mu Wm^{-3}$ are used. The heat production is kept constant inside the individual volumes.

Table 2. Thermal properties reference [2, 19].

Surface Temperature (K)	Ts	273
Lithospheric Basal Flow (Wm^{-2})	q*	0.019
Upper Crust		
Thermal Conductivity ($Wm^{-1}k^{-1}$)	K	3
Radiogenic Heat Production (wm^{-3})	H	1.5×10^{-6}
Lower Crust		
Thermal Conductivity ($Wm^{-1}\ k^{-1}$)	K	2.5
Radiogenic Heat Production (wm^{-3})	H	0.5×10^{-6}
Upper Mantle		
Thermal Conductivity ($Wm^{-1}\ ^{o}k^{-1}$)	K	3
Radiogenic Heat Production (Wm^{-3})	H	0.02×10^{-6}

Elements in the model are all viscoelastic, with viscous behavior controlled by the temperature gradient and the listed constants (Hatzfeld et al [16], Parsons [34], Synder and Barazangi [43], Ni and Barazangi [31]).

7. Boundary Conditions and Loads

The geometry of our model is shown in Figure (3), and the geographical boundaries are superimposed on the topographic map of Figure (1). Our model boundaries are parallel and perpendicular to the Zagros belt trend, i.e extends from North Western Iran (west) near Urumieh to Southeast (East) end of the Zagros (transition zone). It is approximately $1600km \times 600km$.

The first step in running the model was to subject it to gravity, which compressed the model and established an initial stress state. The bottom of the model was constrained to zero displacement in the vertical direction, and the model sides were not permitted to move laterally (fixed in X and Y directions). All other nodes were given 3 degrees of freedom. Elements at the model base mimic low-viscosity, asthenosphere because of high temperatures, see Figure (5). Therefore while compressed, elements at or near the model base could not support any stresses into the upper part of the model, due to the fixed basal boundary condition.

The model edges are oriented parallel and orthogonal to Zagros mountain belt, see Figure (1). Tectonic loading is simulated by moving the western edge of the model according to the convergence rate between Arabia and central Iran. After ~$100ky$ model years, the model reaches a quasi-steady state with nearly constant stresses and strain rates. The results shown below represent the quasi-steady state values.

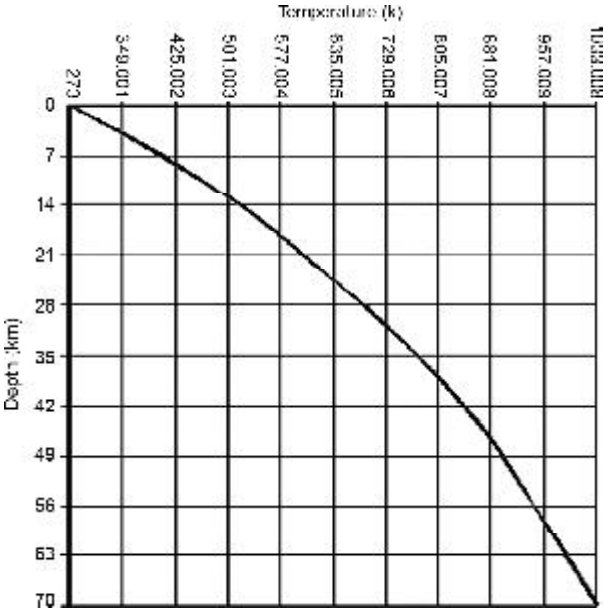

Figure 4. The geothermal gradient used in the model input to the creep equation that controls material behavior. Model elements behave according to Hook's law where temperatures are low and become transitionally more viscoelastic at higher temperatures. Horizontal axis represents the temperature in Kelvin and the vertical axis represents depth in km.

The eastern model edge in *X* and *Y* direction is held fixed due to the central Iran and is thus not free to move laterally. The model base is freely slipping laterally but cannot move vertically. $Ux = 0$ was applied along the left and right short edges of the model.

The model free surface is fully deformable. All velocity constraints are imposed on the model edges as described above and no constraints are imposed on elements within the model. Pore fluid pressure assume hydrostatic.

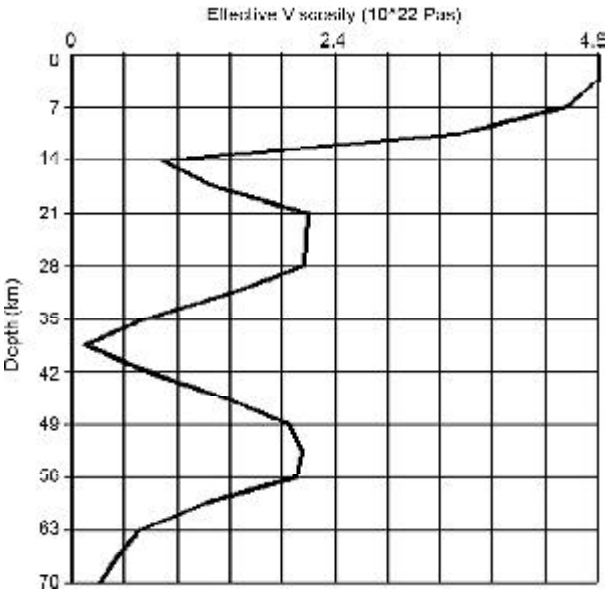

Figure 5. Effective viscosity versus depth. Viscosity is calculated from $n = \sigma^{1-n} \exp(Qc/RT)/2A$, where σ is differential stress (calculated with the finite element model), R is the gas constant, Qc is (activation energy), and A, and n are experimentally determined values, see Table (2). Most of the strength in the model is carried in the crust because a partially wet upper mantle rheology is used. Horizontal axis represents the viscosity in Pa s. Vertical axis represents the depth in km.

8. Model Checking

A simple test for the model (interseismic geodetic observations) was conducted before numerical experiments were used to model tectonic of the area.

Short term geodetic observations measure the interseismic strain field, a combination of the Earth's shallow elastic deformation with the deeper, and ductile response to relative plate motions that occurs while the faults in the seismogenic crust are largely locked. If geodetic observations can be fit, then a degree of confidence in the viscoelastic finite element model is conferred.

To test the Zagros finite element model against geodetic observations, faults were locked from the surface to 20*km* and then the Arabian plate continued to be moved relative to *CIB* for 10 years (providing a span for accurate geodetic observation intervals in Iran). *GPS* velocity field from 3 campaigns in Zagros (north and central) and Kazerun and also in whole Iran [48, 51] were compared with nearest nodes in the finite element model, see Figure (6). Observed and modeled vectors are in reasonable accordance, except in *KSHA* station due to the *GPS* antenna phase center calibration [32, 49], therefore this station was left out from the test.

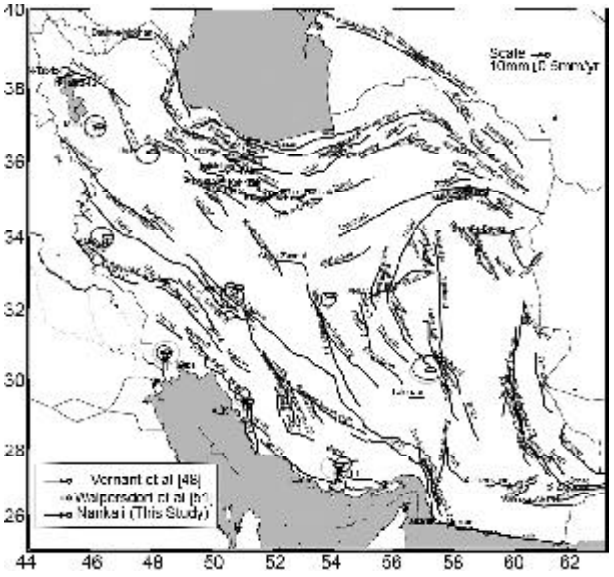

Figure 6. Comparison between model and observed velocity.

9. Numerical Experiments

In principle, the numerical approach would allow the systematic study of the impact of all input parameters as well of the initial and boundary conditions. However, such analysis would go far beyond the scope of this paper. Instead, this work concentrates on the most important parameter influencing the modeling results that is the friction coefficient. Results are presented for steady state of conditions. In all the following numerical experiments the effective fault friction variation is the only parameter that varies. Five experiments were presented and for all of them the effective fault friction is the same in the crust and mantel (case#1: $\mu = 0.02$, case#2: $\mu = 0.05$, case#3: $\mu = 0.1$, case#4: $\mu = 0.2$, case#5: $\mu = 0.3$).

10. Fault Slip Rates (Geological and Geodetical)

In the long-term fault slip rate simulation, the faults were permitted to slip at all depths (0-70*km*). The finite element model was constrained to nearly match

observed long-term fault slip rates within the given error ranges. Long-term fault slip rates derived from geological observations in the Zagros area were compiled by the several workers (eg. [3, 4, 6, 45]). The fault slip rates estimated by model are listed in Table (3). In this study we focus on geodetical and geological slip rates obtained by Walpersdorf [51] and Authemayou et al [3], respectively.

Based on *GPS* measurements a reliable estimate of the present-day dextral strike-slip motion on the Dena is $3.7\pm2 mmyr^{-1}$ and on the Kazerun is $3.6\pm2 mmyr^{-1}$. These segments accommodate the main part of the differential motion between North and Central Zagros. The *MRF GPS* velocity of $2.5\pm2 mmyr^{-1}$ is slower than the Kazerun fault slip rate contrary to the geological slip rates, see Table (3). However, the *GPS* orogen-parallel strike slip motion across the total North Zagros mountain belt is $4\text{-}6 mmyr^{-1}$ [51] and corresponds to the *MRF* geological slip rate. The identification of total horizontal fault displacements and dating of offset alluvial fans by Authemayou et al [3] evaluated geological displacement rates for the Dena and the Kazerun fault segments, to $3.1\text{-}4.7 mmyr^{-1}$ and $1.5\text{-}3.2 mmyr^{-1}$, respectively.

Strictly speaking *GPS* and modeled velocities are not directly comparable, because *GPS* measurements are made during an interseismic period when faults are locked. However, it is usually assumed that the shape of interseismic motions around continental faults is controlled by a locking depth of about 12 to $15 km$ [34, 50]. In this case, the interseismic motion at some distance from the fault (i.e., more than $50 km$) is close to the geological slip rate. Indeed variation of fault slip rate resulting from the change in fault friction only weakly affects the *GPS* site velocities, and fault friction variation does not result in significant velocity changes at the *GPS* sites, and it affects the fault slip rate distribution throughout the model, see Table (4). Therefore, the geologically estimated fault slip rate was used [3, 4, 43] as a control parameter to determine the best model. The estimated model velocity and model slip rate of the each fault in numerical experiments is shown in Table (3).

Table (3) shows the total horizontal fault slips and age of strike slip onsets from Authemayou et al [3] and *GPS* velocities from this study except for *MRF* from Walpersdorf et al [51] in comparison with the model results case#1 ($\mu = 0.02$).

11. Discussion

The 3D visco-elastic finite element model presented here provides a useful tool for simulating long-term lithospheric deformation with faults.

This technique was applied to investigate deformation associated with of major strike-slip faults. Although in this study the focus was put on long-term deformation, this 3*D* visco-elastic model has been developed as a general purpose tool for lithospheric geodynamics. Hence, even though long-term crustal deformation may be adequately simulated with viscoplastic rheology, we kept elastic strain in the model so it can be readily adapted for simulating short-term and transient crustal deformation associated with seismic cycles. The complexity of natural fault geometry, as well as the existence of other active faults in the fault system, can significantly alter the

Table 3. Fault slip rates and velocity estimate from model with $\mu = 0.02$.

Fault	Total Slip [km]	Age of Fault Onset [Ma]	Average Geological Slip Rate [mm/yr]	GPS Velocity [mm/yr]	Finite Element Model (Slip rate) [mm/yr]	Finite Element Model (Velocity) [mm/yr]
Dena	13	2.8-4.2	3.1-4.7	1.7-5.7	4.8	2.8
Kazerun	8.2	2.6-5.5	1.5-3.5	1.6-5.6	2.1	1.9
Borazjan	0	-	-	0-1	0.3-1	0.5
MRF	50	6.6-10.2	4.9-7.6	0.5-4.5	2.3	3.3

Table 4. rms of the residuals velocities and fault slip rates in function of the fault friction.

Experiment	Fault Friction in the Crust	Fault Friction in the Mantel	Velocity Field rms (mm/yr)	Fault Slip Rate rms (mm/yr)
Case#1	0.02	0.02	.8	1.1
Case#2	0.05	0.05	1.0	1.3
Case#3	0.1	0.1	1.1	1.9
Case#4	0.2	0.2	1.4	2.1
Case#5	0.3	0.3	1.5	2.4

patterns of strain localization.

As was mentioned, fault friction variation does not result in significant velocity changes at the *GPS* sites, although it affects the fault slip rate distribution throughout the model. Therefore, the geologically estimated fault slip rates was used as a control parameter to determine the best model, see Table (3). Case#1 gives the highest slip rates on the *MRF* and Kazerun strike-slip faults. On the contrary, case#5 indicates all the faults to be locked. Cases #2 and #3, with intermediate effective fault friction, show intermediate faults slip rates. The comparison between numerical experiments and the geological estimates of the fault slip rates and model velocity suggest that case#1 is the optimal model. In this experiment, the effective fault friction is so low, and frictional fault slip occurs in the lower crust and the upper mantle, see Figure (7). Also, the case #6 was used to check if we can obtain fault slip rates in agreement with the geological estimations without having a discontinuity of the velocity field in the mantle under the crustal faults. In order to do so, an effective fault friction $\mu = 0.02$ was applied in the crust and $\mu = 0.3$ for the extent of the fault down to the mantle. The results of case#6 show much lower velocities than case#1 ($\mu = 0.02$) on the whole fault plane, and are not in agreement with geological estimates.

The identification of total horizontal fault displacements and dating of offset alluvial fans by Authemayou et al [3] enable us to compare the model results with long term average slip rates. For Dena and Kazerun

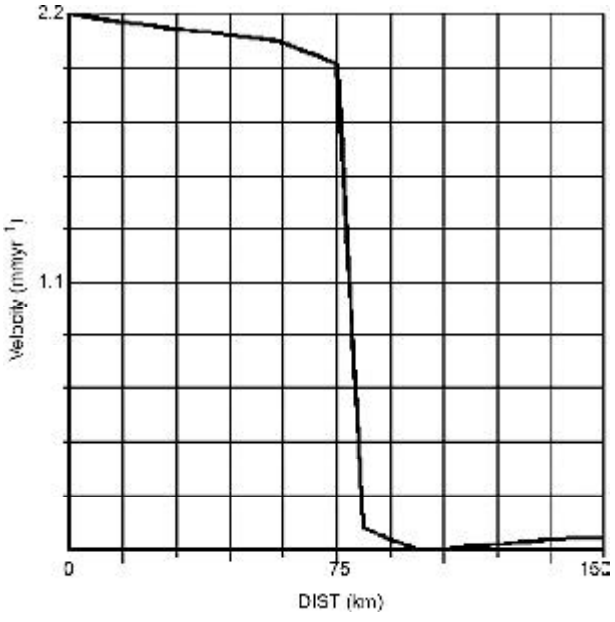

Figure 7. Velocity profile for Kazerun fault in the y direction of the model ($\mu = 0.02$).

fault segments, geological displacement rates are available and evaluated to 3.1-4.7$mmyr^{-1}$ and 1.5-3.2$mmyr^{-1}$, respectively. The comparison of these long term slip rates with the model slip rate shows that the geological and the model results are consistent (within the uncertainties) and less than the 14$mmyr^{-1}$ suggested by Berberian [7]. Assuming a constant slip rate since the onset of the faults and considering the total fault offsets of 13 and 8*km* on the Dena and the Kazerun fault segments, respectively, the coherent long term slip rates yield comparable onset ages for Dena 2.7-4.4*Ma* from model result with respect to 2.8-4.2*Ma* by geology and Kazerun 3.9-4.3*Ma* with respect to 2.6-5.5*Ma* from geology. We do not have a geological onset time for the Borazjan fault, but the model results show that 0.3-1$mmyr^{-1}$ slip rate for this fault as consistent by *GPS*. The Main Recent Fault (*MRF*) trends *NW-SE* and forms the northeastern border of the Zagros Mountains [47]. Long-term Main Recent fault slip rates derived from geological observations in the Zagros area were compiled by several research [e.g. 3, 4, 6, 45]. The geologically estimated fault slip rate [3] was used to determine the best model. The *MRF*, geological displacement rates were evaluated as 4.9-5.7$mmyr^{-1}$. The comparison of this long term slip rate with the model slip rate 2.3$mmyr^{-1}$ and model velocity 3.3$mmyr^{-1}$ shows that the geological and the model results are consistent (within the uncertainties) and less than 10-17$mmyr^{-1}$ suggested by Bachmanov et al [4]. Assuming a constant slip rate since the onset of the faults and considering the total fault offsets of 50*km* on the *MRF*, the coherent long term slip rates yield comparable onset ages for *MRF* 15-21.7*Ma*. There may be two reasons for this, which may have modeled resulting in an apparently lower slip rate on the *MRF*. First, there is uncertainty in the geochronological dating. Second the deformation could not be fully accommodated by strike slip fault, but some is still taken up by the continuum medium.

Indeed, we demonstrated that a variation of the friction coefficient drastically affects the slip rate on faults. The equivalent shear stress change on the fault plane is ~3*MPa* for a seismogenic depth of 10.5*km*.

12. Conclusions

A 3*D* visco-elastic finite element model was developed for simulating lithospheric deformation with faults. In this study this model was adapted to simulate long-term, displacement rates of faults and deformation in the surrounding crust. Our numerical modeling

of the Zagros region allowed us to integrate the forces acting on the lithospheric system in terms of velocity boundary conditions. Indeed, we assigned a very low effective friction on the Kazerun fault and *MRF* (0.02) to reproduce the first-order character of the velocity field. Because the velocity field around and inside the Zagros is well known, the modeling is accurate enough to predict that the upper bound of the effective friction should not be higher than 0.3. Fault slip rates estimated from this model also leads to a very low fault friction in order to fit geological slip rate values. This finding is in good agreement with the low fault friction proposed for some other intracontinental strike-slip faults (e.g., *NAF* and San Andreas fault) and also Vernant and Chéry [50]. In the finite element model a balance of slip between the faults is attained because each fault zone has features that encourage and inhibit slip relative to the others. The *MRF* faults are not ideally aligned with the relative plate motion vector and were given slightly lower slip rate. The Kazerun flexure might absorb more slip (northward increase activity) except that southern termination near Kormuj has lowest slip rate. In summary, an attempt was made to include as much detailed information on crustal structure, rheology, and deformation rates as possible, but calculated results should be interpreted with the caveat of considerable uncertainty.

Acknowledgements

We wish to thank anonymous reviewers for their useful comments and suggestions. Ansys is a trademark of *ANSYS* Inc.

References

1. Allen, M., Jackson, J., and Walker, R. (2004). "Late Cenozoic Reorganization of the Arabia-Eurasia Collision and the Comparison of Short-Term and Long-Term Deformation Rates", *Tectonics*, **23**(2), 16.

2. Artemieva, I.M. and Mooney, D.W. (2001). "Thermal Thickness and Evolution of Precambrian Lithosphere, A Global Study", JGR, **l106**(B8), 16387-16414.

3. Authemayou, C., Chardon, D., Bellier, O., Malekzade, Z., Shabanian, I., and Abbassi, M. (2006). "Late Cenozoic Partitioning of Oblique Plate Convergence in the Zagros Fault-and-Thrust Belt (Iran)", *Tectonics*, **25**(TC3002), doi:10.1029/2005TC001860.

4. Bachmanov, D.M, Trifonov, V.G., Hessami, K., Kozhurin, A.I., Ivanova, P., Rogozhin, E.A., Hademi, M.C., and Jamali, F.H. (2004). "Active Faults in the Zagros and Central Iran", *Tectonophysics*, **380**(3-4), 221-241.

5. Baker, C., Jackson, J., and Priestley, K. (1993). "Earthquakes on the Kazerun Line in the Zagros Mountains of Iran: Strike-Slip Faulting within a Foldand-Thrust Belt", *Geophys. J. Int.*, **115**, 41-61.

6. Berberian, M. (1981). "Active Faulting and Tectonics of Iran, in Zagros-Hindu-Kush-Himalaya Geodynamic Evolution", Eds. Gupta, H.K. and Delany, F.M., Am. Geophys. Union, Geodyn. Ser., **3**, 33-69.

7. Berberian, M. (1995). "Master Blind Thrust Faults Hidden under the Zagros Folds: Active Basement Tectonics and Surface Morphotectonics", *Tectonophysics*, **241**, 193-224.

8. Berberian, M. and King, G.C.P. (1981). "Towards a Paleogeography and Tectonic Evolution of Iran", *Can. J. Earth Sci.*, **18**, 210-265.

9. Bird, P. (1978). "Finite Element Modeling of Lithosphere Deformation: The Zagros Collision Orogeny", *Tectonophysics*, **50**, 307-336.

10. Blanc, E.J.-P., Allen, M.B., Inger, S., and Hassani, H. (2003). "Structural Styles in the Zagros Simple Folded Zone, Iran", *J. Geol. Soc. London*, **160**, 401-412.

11. Byerlee, J.D. (1978). "Friction of Rocks", Pure and Applied Geophysics, **116**, 615-626.

12. Dehghani, G.A. and Makris, J. (1984). "The Gravity Field and Crustal Structure of Iran", N. Jb. Geol. Pal¨aont. Abh., *168*, 215-229.

13. Engdahl, E.R., Jackson, J.A., Stephen, C.M., Bergman, E.A., and Priestley, K. (2006). "Relocation and Assessment of Seismicity in the Iran Region", *Geophys. J. Int.*, **167**, 761-778.

14. Falcon, N. (1974). "Southern Iran: Zagros Mountains, in Mesozoic-Cenozoic Orogenic Belts", ed. Spencer, A.M., Spc. Publ. Geol. Soc. London, **4**, 199-211.

15. Fitch, T.J. (1972). "Plate Convergence, Transcurrent Faults and Internal Deformation Adjacent to Southeast Asia and the Western Pacific", *J. Geophys. Res.*, **77**, 4432-4460.

16. Hatzfeld, D., Tatar, M., Priestley, K., and Ghafory-Ashtiany, M. (2003). "Seismological Constraints on the Crustal Structure Beneath the Zagros Mountain Belt (Iran)", *Geophys. J. Int.*, **155**, 403-410.

17. Haynes, S.J. and McQuillan, H. (1974). "Evolution of the Zagros Suture Zone, Southern Iran", Bull. Geol. Soc. Am., **85**, 739-744.

18. Henk, A. (2006). "Stress and Strain during Fault-Controlled Lithospheric Extension-Insight from Numerical Experiments", *Tectonophysics*, **415**, 39-55.

19. Henk, A. (1997). "Gravitational Orogenic Collapse vs Plate-Boundary Stresses: A Numerical Modelling Approach to the Permo-Carboniferous Evolution of Central Europe, Geol Rundsch" **86**, 39-55.

20. Hessami, K., Koyi, H., Talbot, C.J., Tabasi, H., and Shabanian, E. (2001). "Progressive Unconformities within and Evolving Foreland Fold-Thrust Belt, Zagros Mountains", *J. Geol. Soc. Lond.*, **158**, 969-981.

21. Hessami, K., Nilforoushan, F., and Talbot, C.J. (2006). "Active Deformation within the Zagros Mountains Deduced from GPS Measurements", *J. Geol. Soc. London*, **163**, 143-148.

22. Jackson, J. and McKenzie, D. (1984). "Active Tectonics of the Alpine-Himalayan Belt between Turkey and Pakistan", *Geophysical Journal of the Royal Astronomical Society*, **77**, 185-264.

23. Jackson, J. and Fitch, T. (1981). "Basement Faulting and the Focal Depths of the Larger Earthquakes in the Zagros Mountains (Iran)", *Geophys. J. R. Astr. Soc.*, **64**, 561-86.

24. Jackson, J., Haines, J., and Holt, W. (1995). "The Accommodation of Arabia-Eurasia Plate Convergence in Iran", *J. Geophys. Res.*, **100**, 15 205-15 219.

25. Kaviani, A. (2007). "A Strong Seismic Velocity Contrast in the Shallow Mantle Across the Zagros Collision Zone (Iran)", *Geophys. J. Int.*

26. Kirby, S. (1983). "Rheology of the Lithosphere", Reviews of Geophysics and Space Physics, **21**, 1458-1487.

27. Liu, Z. and Bird, P. (2007). "Kinematic Modelling of Neotectonics in the Persia-Tibet-Burma Orogen", *Geophys. J. Int.*, doi: 10.1111/j.1365-246X.2007.03640.x.

28. McClusky, S.M. (2001). "Present Day Kinematics of the Eastern California Shear Zone form a Geodetically Constrained Block Model", *Geophys. Res. Lett.*, **28**(17), 3369-3372.

29. McQuarrie, N. (2004). "Crustal Scale Geometry of the Zagros Fold-Thrust Belt, Iran", *J. Struct. Geol.*, **26**, 519-535.

30. Molinaro, M., Zeyen, H., and Laurencin, X. (2005). "Lithospheric Structure Underneath the South-Eastern Zagros Mountains, Iran: Recent Slab Break-Off?", TerraNova, **17**, 1-6.

31. Ni, J. and Barazangi, M. (1986). "Seismotectonics of the Zagros Continental Collision and Comparison with the Himalayas", *J. Geophys. Res.*, **91**, 8205-8218.

32. Nilforoushan, F., Masson, F., Vernant, P., Vigny, C., Martinod, J., Abbassi, M., Nankali, H., Hatzfeld, D., Bayer, R., Tavakoli, F., Ashtiani, A., Doeringer, E., Daignie, M., Collard, P., and Chery, J. (2003). "GPS Network Monitors the Arabia-Eurasia Collision Deformation in Iran", *J. of Geodesy*, **77**, 411-422.

33. Parsons, T., Bruns, T.R, and Sliter, R. (2005). "Structure and Mechanics of the San Andreas-San Gregorio Fault Junction", San Francisco, California, *Geochem. Geophys. Geosyst.*, **6**, Q01009, doi:10.1029/2004GC000838.

34. Parsons, T. (2002). "Post-1906 Stress Recovery of the San Andreas Fault System Calculated from Three-Dimensional Finite Element Analysis", *J. of Geophysical Research*, **107**(B8), 10.1029/2001JB001051, 2002.

35. Parsons, T. (2006). "Tectonic Stressing in California Modeled from GPS Observations", *J. Geophys. Res.*, **111**, B03407, doi:10.1029/2005JB003946.

36. Paul, A., Kaviani, A., Hatzfeld, D., Vergne, J., and Mokhtari, M. (2006). "Seismological Evidence for Crustal-Scale Thrusting in the Zagros Mountain Belt (Iran)", *Geophys. J. Int.*, doi: 10.1111/j.1365-246X.2006.02920.x.

37. Reilinger, R., McClusky, S., Vernant, P., Laurence, S., Ergintav, S., Cakmak, R., Ozener, H., Kadirov, F., Guliev, I., Stepanyan, R., Nadariya, M., Hahubia, G., Mahmoud, S., ArRajehi, A., Abdulaziz, K., Paradissis, D., Al-Aydrus, A., Prilepin, M., Guseva, T., Evren, E., Dmitrotsa, A., Filikov, S.V., Gomez, F., Al-Ghazzi, R., and Karam, G. (2006). "GPS Constraints on Continental Deformation in the Africa-Arabia-Eurasia Continental Collision Zone and Implications for the Dynamics of Plate Interactions", *J. Geophys. Res.*, **111**(B5), doi: 10.1029/2005JB004051.

38. Sella, G.F., Dixon, T.H., and Mao, A. (2002). "REVEL: A Model for Recent Plate Velocities from Space Geodesy", *J. Geophys. Res.*, **107**(B4), ETG 11-1, 11-32.

39. Sherkaty, S. and Letouzey, J. (2004). "Variation of Structural Style and Basin Evolution in the Central Zagros (Izeh Zone and Dezful Embayment), Iran", Marine and Petroleum Geology, **21**(5), 535p.

40. Stocklin, J. (1974). "Possible Ancient Continental Margin in Iran", In Geology of Continental Margins, Eds Burke, C. and Drake, C., Springer-Verlag, NewYork, 873-877.

41. Stoneley, R. (1981). "The Geology of the Kuh-e-Dalneshin Area of Southern Iran, and Its Bearings on the Evolution of Southern Thetys", *J. Geol. Soc. Lond.*, **138**, 509-526.

42. Sobouti, F. and Arkani-Hamed, J. (1996). "Numerical Modelling of the Deformation of the Iranian Plateau", *Geophys. J. Int.*, **126**, 805-818.

43. Synder, D.B. and Barazangi, M. (1986). "Deep Crustal Structure and Flexure of the Arabian Plate Beneath the Zagros Collisional Mountain Belt as Inferred from Gravity Observations", *Tectonics*, **5**, 361-373.

44. Talebian, M. and Jackson, J. (2002). "Offset on the Main Recent Fault of the NW Iran and Implications on the Late Cenozoic Tectonics of the Arabia-Eurasia Collision Zone", *Geophys. J. Int.*, **150**, 422-439.

45. Talebian, M. and Jackson, J. (2004). "A Reappraisal of Earthquake Focal Mechanisms and Active Shortening in the Zagros Mountains of Iran", *Geophys. J. Int.*, **156**, 506-526.

46. Tatar, M., Hatzfeld, D., Martinod, J., Walpersdorf, A., Ghafory-Ashtiany, M., and Chéry, J. (2002). "The Present-Day Deformation of the Central Zagros from GPS Measurements", Geophys. Res. Lett., **29**(19), 1927.

47. Tatar, M., Hatzfeld, D., and Ghafory-Ashtiany, M. (2004). "Tectonics of the Central Zagros (Iran) Deduced from Microearthquake Seismicity", *Geophys. J. Int.*, **156**, 255-266.

48. Vernant, P., Nilforoushan, F., Hatzfeld, D., Abbassi, M.R.,Vigny, C., Masson, F., Nankali, H., Martinod, J., Ashtiani, A., Bayer, R., Tavakoli, F., and Chery, J. (2004). "Present-Day Crustal Deformation and Plate Kinematics in the Middle East Constrained by GPS Measurements in Iran and Northern Oman", *Geophys. J. Int.*, **157**, 381-398.

49. Vernant, P. and Chéry, J. (2006). "Mechanical Modelling of Oblique Convergence in the Zagros, Iran", *Geophys. J. Int.*, **165**, 991-1002.

50. Vernant, P. and Chéry, J. (2006). "Low Fault Friction in Iran Implies Localized Deformation for the Arabia-Eurasia Collision Zone", Earth and Planetary Science Letters, **246**, 197-206.

51. Walpersdorf, A., Hatzfeld, D., Nankali, H.R., Tavakoli, F., Nilforoushan, F., Tatar, M., Vernant, P., Chery, J., and Masson, F. (2007). "Difference in the GPS Deformation Pattern of North and Central Zagros (Iran)", *Geophys. J. Int.*, doi: 10.1111/j.1365-246X.2006.03147.x.

52. Wilcox, R.E., Harding, T.P., and Seely, D.R. (1973). "Basic Wrench Tectonics", AAPG Bulletin, **57**, 74-96.C_ 2006, The Authors, GJI.